Synthesis of Poly(*n*-butyl acrylate)-*block*-poly(acrylic acid) Diblock Copolymers by ATRP and Their Micellization in Water

Olivier Colombani,[†] Markus Ruppel,[†] Frank Schubert,[‡] Heiko Zettl,[‡] Dmitry V. Pergushov,[§] and Axel H. E. Müller*,[†]

Makromolekulare Chemie II, Physikalische Chemie II, and Bayreuther Zentrum für Kolloid- und Grenzflächenforschung, Universität Bayreuth, D-95440 Bayreuth, Germany, and Department of Polymer Science, Faculty of Chemistry, Moscow State University, Vorob'evy Gory, Moscow 119992, Russia

Received April 30, 2006; Revised Manuscript Received March 29, 2007

ABSTRACT: Amphiphilic diblock copolymers, poly(*n*-butyl acrylate)-*block*-poly(acrylic acid) (P*n*BA-PAA), with narrow molecular weight distribution (PDI ≤ 1.07) were prepared by atom transfer radical polymerization (ATRP) of *n*-butyl acrylate and *tert*-butyl acrylate (*t*BA), followed by selective acidolysis of the P*t*BA block. These polymers possess a soft P*n*BA hydrophobic block with a constant chain length of 90−100 monomer units and pH- and ionic strength-sensitive hydrophilic PAA block with DP_{PAA} = 33−300 AA monomer units. They were expected to form stimuli-responsive micelles. The block copolymers with $DP_{PAA} \geq 100$ are directly soluble in water at pH > 4.7. Pyrene steady-state fluorescence spectroscopy and fluorescence correlation spectroscopy (FCS) studies indicate the existence of a very low critical micelle concentration (cmc ∼ 10^{-8} mol/L). The number-average hydrodynamic radii of the micelles, as determined by FCS, range from 28 to 55 nm, depending on the PAA block length. FCS data indicate that micellar sizes significantly decrease upon dilution for salt-free systems. This is attributed to a dynamic, but kinetically controlled, behavior of these self-assembled nanostructures. In saline solutions the micellar sizes remain constant above the "apparent" cmc (cmc*), which is attributed to slower dynamics of unimer exchange between micelles.

Introduction

Amphiphilic block copolymers may self-assemble into a wide range of supramolecular structures such as spherical micelles, rods, or vesicles,[1−7] which are of interest in a number of fields: drug delivery,[8−10] removal of pollutants from water, or stabilization of emulsion polymerization,[11,12] for example. Among the systems developed, the most interesting ones are stimuli-responsive micelles, which may change their physical parameters (shape, aggregation number, size, etc.) in response to external stimuli, such as pH, ionic strength, or temperature. These micelles must be "dynamic"; i.e., they are in equilibrium with their unimers (single block copolymer chains), similar to low-molecular-weight surfactants. Here, the unimer exchange enables the formation of monodisperse and well-defined self-assembled supramolecular structures. However, most of the polymeric amphiphiles developed up to now possess a hydrophobic core having a high glass transition temperature, T_g (e.g., polystyrene), and thus form nondynamic, "frozen" micelles.[13−20] Those micelles are not in equilibrium with their unimers as unimer exchange is hindered due to kinetic constraints. As one of the consequences, they have to be dissolved in aqueous media with the help of a nonselective cosolvent or by heating above the T_g of the hydrophobic block. An exception to this rule is when the (nonequilibrium) micellar structure has already preformed in the bulk, as was shown for polystyrene-*block*-poly(acrylic acid) (PS−PAA).[21,22] Here, the corresponding self-organized bulk films dissolve spontaneously in water and form nonequilibrium assembled structures reminiscent of those obtained in the bulk phase. Rather recently, dynamic micelles were obtained from block copolymers having a soft hydrophobic block. For example, polyisobutylene-*block*-poly(methacrylic acid) (PIB−PMAA), having a hydrophobic PIB block of short to medium length (degree of polymerization, DP_{PIB} = 25−75) and a long PMAA hydrophilic block (DP_{PMAA} > 100), appears to form dynamic micelles.[23,24] Owing to the low T_g of the PIB block (T_g ∼ −65 °C), these polymers are spontaneously soluble in water (at pH > 7 for $DP_{PIB} \leq 75$) and yield micelles sensitive to different stimuli (pH, ionic strength). On the contrary, the same PIB−PMAA diblock copolymers were brought into water using THF as a cosolvent when the PIB block becomes too long or comparable in length with the PMAA block (PIB_{70}−$PMAA_{50-70}$ or PIB_{134}−$PMAA_{150-300}$).[25] Polyethylethylene-*block*-poly(styrenesulfonic acid) (PEE−PSS) with DP_{PEE} = 114 and DP_{PSS} = 83 is also directly soluble in water, forming micellar aggregates.[26]

We thus decided to focus on block polymers that consist of a soft hydrophobic block similar in length, but which are less hydrophobic in nature, in order to assess whether dynamic micelles can be obtained with such a system.

The polymer chosen was poly(*n*-butyl acrylate)-*block*-poly(acrylic acid) (P*n*BA−PAA). The P*n*BA block is less hydrophobic than PIB or PEE, and its PAA block is more hydrophilic than PMAA due to the absence of the hydrophobic α-methyl group. Gaillard et al. reported the synthesis of P*n*BA−PAA diblock copolymers by sequential monomer addition using radical addition fragmentation transfer (RAFT) polymerization.[12] Since the second monomer (*n*BA) was directly added after only 61−94% conversion of the acrylic acid and without purification of the first block, this resulted in less defined polymers with high polydispersity (PDI = 1.4−2.3) and only short P*n*BA and PAA blocks (DP < 50). More importantly, the P*n*BA block contained a considerable fraction of AA units. The incorporation of AA units into the hydrophobic block of an amphiphilic block

* To whom correpondence should be addressed: Ph +49-921-553399, Fax +49-921-553393; e-mail axel.mueller@uni-bayreuth.de.
[†] Makromolekulare Chemie II, Universität Bayreuth.
[‡] Physikalische Chemie II, Universität Bayreuth.
[§] Moscow State University.

10.1021/ma0609578 CCC: $37.00
Published on Web 05/16/2007

Table 1. Experimental Conditions for the Synthesis of the Precursors and Block Copolymers by ATRP

	T (°C)	initiator	[M]:[I]:[Cu(I)]:[Cu(II)]:[L]	monomer/solvent[b]/ decane (wt %)	reaction time (h)	final conv (%)
P*n*BA$_{90}$-Br	60	MBP	200:1:0.5:0:0.5	70/23/7	8.25	45
P*n*BA$_{100}$-Br	77	EBIB	140:1:2:0:2	26/71/3	4.75	70
P*n*BA$_{90}$−P*t*BA$_{33}$	40−60[a]	P*n*BA$_{90}$-Br	60:1:0.5:0.025:0.5	70/23/7	25	55
P*n*BA$_{90}$−P*t*BA$_{100}$	60	P*n*BA$_{90}$-Br	200:1:0.5:0.025:0.5	70/23/7	68	50
P*n*BA$_{100}$−P*t*BA$_{150}$	60	P*n*BA$_{100}$-Br	200:1:0.5:0:0.5	70/23/7	61.5	58
P*n*BA$_{90}$−P*t*BA$_{300}$	60	P*n*BA$_{90}$-Br	600:1:0.5:0.05:0.5	70/23/7	16 days	50

[a] The polymerization was started at 40 °C, and the temperature was raised to 60 °C after 17.25 h. [b] Acetone was used as solvent for all polymerizations, except for P*n*BA$_{100}$-Br where ethyl acetate was chosen.

copolymer dramatically changes the physicochemical properties of the copolymers, as was recently shown by Bendejacq et al. for PS−PAA.[27]

In order to obtain block copolymers whose structure was better controlled for our purpose, we turned toward atom transfer radical polymerization (ATRP), which allows reaching high degrees of polymerization with a good control of functionality and polydispersity. In this first paper, we report the synthesis of diblock copolymers having a well-defined block character, a low polydispersity index (PDI < 1.1), and a long P*n*BA block of almost constant length (degree of polymerization, DP = 90−100). Their solubilization and micelle formation was studied by potentiometric titration, steady-state fluorescence spectroscopy, and fluorescence correlation spectroscopy (FCS), indicating that micelles are indeed obtained by dissolving the polymers in water at pH > 4.7 without the help of any cosolvent. A complete characterization of the micelles as a function of different parameters, such as pH, ionic strength, preparation conditions, or PAA length, is the subject of a subsequent paper.[24]

Experimental Section

1. Synthesis. Materials. *n*-Butyl acrylate and *tert*-butyl acrylate (kindly supplied by BASF AG) were stirred overnight on calcium hydride (Merck, 95%) with Irganox 1010 inhibitor (CIBA Geigy), distilled under vacuum, and degassed by three freeze/pump/thaw/flood with nitrogen cycles. CuBr (Aldrich, 98%) was stirred overnight in glacial acetic acid, filtered, and rinsed successively by acetic acid, ethanol, and ether to remove traces of $CuBr_2$.[28] *N*,*N*,*N*′,*N*′,*N*″-Pentamethyldiethylenetriamine (PMDETA, Aldrich, 98%), ethyl 2-bromoisobutyrate (EBIB, Aldrich, 98%), and methyl-2-bromopropionate (MBP, Aldrich, 98%) were distilled (under vacuum if necessary) and degassed by freeze/thaw cycles. Ethyl acetate (Merck, >98%), acetone (Merck, 99.8%), and *n*-decane (99%+, Aldrich) were degassed by freeze/thaw cycles. Neutral Al_2O_3 (Ecochrom), SiO_2 (63−200 μm, Merck), methanol (Merck, 99.8%), THF (Merck, 99.8%), trifluoroacetic acid (CF_3COOH, Merck, >99%), and dichloromethane (Aldrich, 99.8%) were used as received.

Macroinitiators. For the macroinitiator P*n*BA$_{90}$-Br, a single-neck 500 mL flask was filled in a glovebox with Cu(I)Br (0.6152 g, 4.29 × 10^{-3} mol), *n*BA (220.0 g, 1.72 mol), acetone (73.3 g), *n*-decane (22.0 g), and PMDETA (0.7415 g, 4.28 × 10^{-3} mol). After complete dissolution of the Cu(I)Br/PMDETA complex, a few drops of the solution were taken as sample t_0. Methyl 2-bromopropionate (1.435 g, 8.59 × 10^{-3} mol) was then added, the flask was closed with a septum, taken out of the glovebox, and dipped in an oil bath at 60 °C. Samples were taken under nitrogen flow throughout the reaction to follow the kinetics. The samples were cooled immediately in an ice/water bath and opened to air. A few drops of the sample were diluted in several milliliters of THF and injected in gas chromatography (GC) to determine the conversion using *n*-decane as internal standard. The conversion of monomer at time *t* is $x_P = 1 - A_t/A_0$, where A_t and A_0 are the ratios of the monomer to *n*-decane peaks in the GC, respectively, at times *t* and t_0. Some drops of the sample were also diluted with 0.5 mL of $CDCl_3$ in order to determine the conversion by ^{1}H NMR spectroscopy using the peaks at 4 ppm (−OCH_2− both of the polymer and of the monomer) and between 5.5 and 6.5 ppm (CH_2=CH− of the monomer). The samples were further characterized by SEC and MALDI-TOF MS after removal of the copper complex by flash chromatography on a small SiO_2 column.

The reaction was finally terminated at 45% conversion by cooling the flask to 0 °C (ice−water) and opening it to the atmosphere. The copper complex was removed by flash chromatography on a two-layer Al_2O_3/SiO_2 column rinsed with chloroform and acetone, removal of most of the residual monomer and solvent by rotating evaporation, and precipitation at −40 °C in methanol. Efficient precipitation of the polymer was achieved by keeping the polymer/methanol solution overnight at −40 °C. The polymer was then collected by decantation of the supernatant. After three purifications in that way, and removal of the residual solvent under vacuum, a viscous colorless polymer (87.7 g, 89% yield) was finally obtained. M_n(theoretical) = 11 700 g/mol; GPC (THF): M_n = 12 800 g/mol, PDI = 1.08; MALDI-TOF MS: M_n = 12 900 g/mol, PDI = 1.13. ^{1}H NMR (250 MHz, $CDCl_3$): δ (ppm) = 4.04 (t, ^3J(H,H) = 5 Hz, 2H, O−CH_2−), δ = 2.28 (m, 1H, −CH_2−C(C=O)H−), δ = 1.90 and hidden under the other signals between 1.2 and 1.7 (m, 2H, −CH_2−C(C=O)H−), δ = 1.60 (m, 2H, O−CH$_2$−CH_2−CH$_2$−CH$_3$), δ = 1.35 (m, 2H, O−CH$_2$−CH$_2$−CH_2−CH$_3$), δ = 0.93 (t, ^3J(H,H) = 5 Hz, 3H, O−CH$_2$−CH$_2$−CH$_2$−CH_3). ^{13}C NMR (50 MHz, [D$_8$]THF): δ (ppm) = 175.0 (*C*=O), δ = 64.8 (O−*C*H$_2$−CH$_2$−CH$_2$−CH$_3$), δ = 42.4 (−CH$_2$−*C*(C=O)H−), δ = 36.0 (−*C*H$_2$−C(C=O)H−), δ = 31.7 (O−CH$_2$−*C*H$_2$−CH$_2$−CH$_3$), δ = 20.1 (O−CH$_2$−CH$_2$−*C*H$_2$−CH$_3$), δ = 14.2 (O−CH$_2$−CH$_2$−CH$_2$−*C*H$_3$). The precursor P*n*BA$_{100}$-Br was synthesized in a similar way. For conditions see Table 1 and Supporting Information.

Diblock Copolymers. The diblock copolymers were prepared by ATRP under similar conditions as for the precursor, by using P*n*BA$_{90}$-Br and P*n*BA$_{100}$-Br as macroinitiators for the polymerization of the P*t*BA block. The experimental conditions for the synthesis of each second block are summarized in Table 1. For these reactions, 0−10% $CuBr_2$ (relative to CuBr) was added to the reaction mixture to decrease termination reactions. This latter component was dissolved separately in acetone and PMDETA and then added when the other reagents were solubilized. Kinetics were followed by gas chromatography, MALDI-TOF MS spectroscopy, and size exclusion chromatography. Purification of the shortest diblocks was similar to that of the first block. The polymers having the longest P*t*BA blocks are soft solids and were ultimately freeze-dried in dioxane for better removal of residual solvent. As an example, the ^{1}H NMR (250 MHz, $CDCl_3$) characterization of P*n*BA$_{90}$−P*t*BA$_{300}$ is given: δ (ppm) = 4.03 (t, ^3J(H,H) = 5 Hz, 2H P*n*BA, O−CH_2−), δ = 2.24 (m, 1H P*n*BA and 1H P*t*BA, −CH_2−C(C=O)H−), δ = 1.83 and hidden under the other signals between 1.2 and 1.7 (m, 2H P*n*BA and 2H P*t*BA, −CH_2−C(C=O)H−), δ = 1.56 (m, 2H P*n*BA, O−CH$_2$−CH_2−CH$_2$−CH$_3$), δ = 1.44 (m, 9H P*t*BA, O−C(CH_3)$_3$), δ = 1.35 (m, 2H P*n*BA, O−CH$_2$−CH$_2$−CH_2−CH$_3$), δ = 0.94 (t, ^3J(H,H) = 5 Hz, 3H P*n*BA, O−CH$_2$−CH$_2$−CH$_2$−CH_3). ^{13}C NMR (50 MHz, [D$_8$]THF): δ (ppm) = 174.6 (*C*=O, P*n*BA and P*t*BA), δ = 80.8 (O−*C*(CH$_3$)$_3$, P*t*BA), δ = 64.8 (O−*C*H$_2$−CH$_2$−CH$_2$−CH$_3$, P*n*BA), δ = 43.1 (−CH$_2$−*C*(C=O)H−, P*n*BA and P*t*BA), δ = 36.8 (−*C*H$_2$−C(C=O)H−, P*n*BA and P*t*BA), δ = 31.8 (O−CH$_2$−*C*H$_2$−CH$_2$−CH$_3$,

P*n*BA), $\delta = 28.5$ (O−C(CH_3)$_3$, P*t*BA), $\delta = 20.1$ (O−CH_2−CH_2−CH_2−CH_3, P*n*BA), $\delta = 14.3$ (O−CH_2−CH_2−CH_2−CH_3, P*n*BA).

The synthesis of P*n*BA$_{100}$−P*t*B$_{150}$ is similar to that of the three other block copolymers. However, the copolymer contained some residual homopolymer (P*n*BA$_{100}$) because some P*n*BA-Br macroinitiator chains had been deactivated (either by dehydrobromination or by termination by disproportionation). After acidolysis of the unpurified P*n*BA$_{100}$−P*t*BA$_{150}$, Soxhlet extraction in cylohexane yielded pure P*n*BA$_{100}$−PAA$_{150}$. Details are given in the Supporting Information.

Acidolysis of P*n*BA−P*t*BA to P*n*BA−PAA. The P*n*BA−P*t*BA diblock copolymers were dissolved in dichloromethane ($c \sim 150$ g/L) and stirred at room temperature for 48 h with 5 equiv of trifluoroacetic acid relative to the amount of *t*BA units. The polymers did not precipitate and were collected after rotating evaporation of the solvent and the trifluoroacetic acid. Further elimination of the residual CF_3COOH was achieved in the case of P*n*BA$_{90}$−PAA$_{33}$ by two cycles of redissolution in dichloromethane/methanol (10/1 v/v), rotating evaporation, and vacuum pumping overnight. For P*n*BA$_{90}$−PAA$_{100}$ and P*n*BA$_{90}$−PAA$_{300}$, the traces of trifluoroacetic acid were removed by freeze-drying in dioxane/methanol (40/1 v/v). Elemental analysis of traces of fluorine (performed on one sample), as well as ^{13}C NMR, revealed the absence of significant quantities of residual trifluoroacetic acid after drying. As an example, the NMR characterization of P*n*BA$_{90}$−PAA$_{300}$ is given. ^{1}H NMR (250 MHz, MeOD): δ (ppm) = 4.09 (t, 2H P*n*BA, O−CH_2−), $\delta = 2.44$ (m, 1H PAA, −CH_2−C(C═O)-H−), $\delta = 2.32$ (m, 1H P*n*BA, −CH_2−C(C═O)H−), $\delta = 1.93$ and hidden under the other signals between 1.3 and 1.8 (m, 2H P*n*BA and 2H PAA, −CH_2−C(C═O)H−), $\delta = 1.65$ (m, 2H P*n*BA, O−CH_2−CH_2−CH_2−CH_3), $\delta = 1.44$ (m, 2H P*n*BA, O−CH_2−CH_2−CH_2−CH_3), $\delta = 0.98$ (t, 3H P*n*BA, O−CH_2−CH_2−CH_2−CH_3). Integration of the protons between 0.7 and 2.8 ppm (20.7H when the −OCH_2 peak of P*n*BA at 4.09 ppm is fixed to 2H) is close to the theoretical value for complete hydrolysis (3H PAA + 10H P*n*BA = 20.0H), which reveals a degree of hydrolysis close to 100%. ^{13}C NMR (62.5 MHz, [D8]THF): δ (ppm) = 177.2 (*C*═O, PAA), $\delta = 175.0$ (*C*═O, P*n*BA), $\delta = 64.8$ (O−*C*H_2−CH_2−CH_2−CH_3, P*n*BA), $\delta = 42.4$ (−CH_2−*C*(C═O)H−, P*n*BA and PAA), $\delta = 36.0$ (−*C*H_2−C(C═O)H−, P*n*BA and PAA), $\delta = 31.8$ (O−CH_2−*C*H_2−CH_2−CH_3, P*n*BA), $\delta = 20.1$ (O−CH_2−CH_2−*C*H_2−CH_3, P*n*BA), $\delta = 14.2$ (O−CH_2−CH_2−CH_2−*C*H_3, P*n*BA).

Molecular Characterization. For gas chromatography, samples diluted in THF were injected at a temperature of 250 °C on a Fisons GC 8000 system gas chromatograph. A Megabore methylpolysiloxane capillary column DB1 (length: 30 m, 0.53 mm i.d., film thickness 1.5 μm) was employed as stationary phase and hydrogen as mobile phase. Separation for the determination of the conversion of both *n*BA and *t*BA was performed using the following temperature program: 2 min at 60 °C, heating at 20 °C/min up to 120 °C, and keeping at 120 °C until the end of the experiment. The components were detected with a flame ionization detector operating at 250 °C. Raw data were recorded and evaluated using the ChromCard for Windows Software V1.17β.

^{1}H and ^{13}C NMR spectra were recorded on a Bruker AC 250 NMR spectrometer with samples dissolved in $CDCl_3$, $CDCl_3$/MeOD (85/15 v/v), MeOD, or [D_8]THF, and spectra were treated using the WinNMR program. Calibration of the spectra was made either by adding some tetramethylsilane in the NMR tube ($\delta = 0$ ppm) or by using the solvent residual peak as reference.

Size exclusion chromatography (SEC) was performed with PSS SDV-gel columns (5 μm, 60 cm, 1 × linear (10^2−10^5 Å), 1 × 100 Å) with THF as eluent (flow rate = 1.0 mL/min), at room temperature, and using UV spectrometry ($\lambda = 230$ and 260 nm) and refractometry for detection. The number-average molecular weight (M_n) and molecular weight distribution (MWD) were determined using polystyrene standards calibration. For MALDI-TOF mass spectrometry, samples were prepared by mixing the polymer, the matrix (3-indoleacrylic acid), and the salt (NaI) in THF (proportion 1:10:1), and evaporating the solution on a grid. The samples were analyzed using a Bruker Reflex III spectrometer operating in linear mode.

2. Characterization in Solution. Reagents. The aqueous solutions were prepared using Millipore water (deionized water, resistance >18 MΩ), sodium chloride (99.5%, Fluka), tris(2-amino-2-hydroxymethyl-1,3-propanediol) (TRIS, Aldrich, 99.8%), HCl (0.01, 0.1, or 1 M), and NaOH (0.01, 0.1, or 1 M). NaOH and HCl solutions were prepared using Titrisol concentrated solutions, and NaOH solutions were back-titrated with HCl before use. Pyrene (Aldrich, 98%), rhodamine 6G perchlorate (Lamda Physik), and octadecyl rhodamine B (Sigma-Aldrich) were used as fluorescent probes without further purification. pH was measured using a glass electrode connected to a Schott pH-meter CG 840 calibrated with two buffers solutions at pH 4.0 and 10.0. A third buffer at pH 7.0 was used to check the accuracy of the pH-meter.

Potentiometric Titrations were performed at room temperature with an automatic titrator (Titrando 806, Metrohm) controlled by the Metrohm Tiamo computer software. The combined glass electrode (Unitrode Pt1000, 6.0258.000, Metrohm) was calibrated using three different pH buffers (pH 4.01, 7.00, and 9.00, Merck CertiPUR) prior to each measurement. Sample solutions were prepared by dissolving the polymers at 1.0 g/L and pH ~ 11 in the absence of salt and adding 0.1 M NaCl after at least one night of stirring to ensure complete dissolution of the polymer. After 24 h of equilibration, a known volume of the polymer solution (~10 mL) was added to the jacked glass cell of the titrator and titrated by an aqueous HCl solution (0.1 M HCl and 0.1 M NaCl) using a 2 mL buret (Dosing unit 807, Metrohm) driven by a Metrohm Dosino 800. Measurements were started after 5 min of equilibration and with volume increments of 5−50 μL spaced by at least 180 s (a drift of 5 mV/min was applied). The equivalence points of the titration (the first one corresponding to the titration of the excess NaOH, the second one to the complete protonation of PAA^-,Na^+) were set as the inflection points (maximum of the first derivative).

Pyrene Fluorescence Spectroscopy.[23,29,30] A stock solution of the polymer was first prepared at a concentration of 10^{-4} mol/L and pH ~ 9−10 ($\alpha \sim 1$) by dissolving the polymer in water with 1 equiv of NaOH compared to the AA units. After complete dissolution of the polymer, 0.1 M NaCl and 0.01 M TRIS were added. The latter was used to keep the pH constant during the successive dilutions of the polymer solutions. The advantage of TRIS is that it is a very efficient buffer even at low concentration and thus does not significantly change the ionic strength of the solution or the emission/absorption pyrene spectra. The polymer stock solution was then diluted to 10 different concentrations down to 10^{-10} mol/L using a buffer solution of water containing 0.01 M TRIS and 0.1 M NaCl. Each sample was then prepared by dropping carefully 60 μL of a pyrene solution (2.5×10^{-5} mol/L in acetone) into an empty vial, evaporating the acetone by gentle heating at 50−60 °C, adding 3 mL of one of the polymer solutions, and stirring the closed and light-protected vials 48−72 h at 50−60 °C. The final concentration of pyrene in water thus reached 5×10^{-7} mol/L, which is slightly below the pyrene saturation concentration in water at 22 °C. Polymer solutions were also prepared in the same manner without added salt or TRIS.

Steady-state fluorescence spectra of the air-equilibrated samples were recorded with a Shimadzu RF-5301 PC spectrofluorophotometer (right angle geometry, 1 cm × 1 cm quartz cell) using the following conditions: excitation at 333 nm, slit width 3 nm for the excitation, and 1.5 nm for the emission. The intensities of the bands I_1 at 372 nm and I_3 at 383 nm were then evaluated, and their ratio was plotted vs the polymer concentration.

Fluorescence Correlation Spectroscopy (FCS). Aqueous solutions at polymer concentrations ranging from 2.25×10^{-2} to 1×10^3 mg/L were prepared in glass vials from a stock solution made by dissolving the polymer in the absence of added salt at pH ~ 9.5 (degree of ionization $\alpha = 1$) and 1 g/L. This stock solution was further diluted to the desired concentrations with alkaline water at pH ~ 9.5. After one night of equilibration 100 mL of the fluorescent dye, either rhodamine 6G perchlorate (Rh6G), c_1(Rh6G) = 2.0×10^{-7} mol/L, c_2(Rh6G) = 1.1×10^{-8} mol/L, or octadecyl rhodamine

B (ORB), $c(\text{ORB}) = 1.0 \times 10^{-8}$ mol/L, was added to 900 mL of each polymer solution, resulting in the final concentrations of the fluorescent probe $c_{1,0}(\text{Rh6G}) = 2.0 \times 10^{-8}$ mol/L, $c_{2,0}(\text{Rh6G}) = 1.1 \times 10^{-9}$ mol/L, and $c_0(\text{ORB}) = 1.0 \times 10^{-9}$ mol/L. Measurements were performed at least 24 h after dilution of the micellar solutions on a ConfoCorII setup (Carl Zeiss Jena). An argon ion laser was applied for excitation of the dye molecules at $\lambda_1 = 488$ nm and $\lambda_2 = 514$ nm. The laser beam was focused by a C-Apochromat 40× water immersion objective (numerical aperture of 1.2). Measurements were taken in typical sample volumes of 35 μL. The emitted fluorescent light was collected by the same objective and separated from the excitation light by a dichroic mirror. The emission beam was mapped onto a pinhole in the image plane of the objective (70 μm at λ_1 and 74 μm at λ_2). Fluorescence was detected by an avalanche photodiode in single-photon-counting mode. Further information about the setup for FCS is given elsewhere.[31,32]

The translational diffusion time and the number of fluorescent particles in the illuminated volume (the confocal volume, V_c) are obtained from the autocorrelation function of the intensity fluctuations monitored as a function of time. For polydisperse systems those values have to be regarded as number averages.

Fluorescence fluctuations may arise from phenomena such as Brownian diffusion, flow, and chemical reaction. When the fluorescence fluctuations are only a consequence of diffusive processes through the illuminated volume—being regarded as an ellipsoid with radius w_{xy} and focus length $2w_z$—and provided that the quantum efficiency of the dye molecules does not change upon binding to the micelles, the autocorrelation function $G(\tau)$ (ACF) may be derived in an analytical form as

$$G(\tau) = 1 + \frac{\frac{T}{1-T}e^{-\tau/\tau_{tr}}}{\bar{N}} \sum_{i=1}^{K} \frac{\phi_i}{1+\frac{\tau}{\tau_i}} \frac{1}{\sqrt{1+\frac{\tau}{S^2\tau_i}}} \quad (1)$$

where K is the number of fluorescent probes with different diffusion characteristics, τ_i is the averaged time needed by the fluorescent particle of fraction i to pass the illuminated volume, and T denotes the fraction of dye molecules in the triplet state with lifetime τ_{tr}. $\bar{N}$ is assigned to the averaged number of fluorescent particles within the excitation volume, and ϕ_i is the fraction of the ith component.[33,34] S denotes the geometry parameter of the confocal volume, defined as the ratio of the focus length and radius

$$S = \frac{w_z}{w_{xy}} \quad (2)$$

The translational diffusion coefficients, D_i, are related to the respective diffusion times by

$$D_i = \frac{w_{xy}^2}{4\tau_i} \quad (3)$$

The hydrodynamic radii, $R_{h,i}$, are given by the Stokes−Einstein equation

$$R_{h,i} = \frac{k_B T}{6\pi\eta_0 D_i} \quad (4)$$

with k_B the Boltzmann constant, T the absolute temperature, and η_0 the solvent viscosity.

All experiments were performed at ambient temperature without further temperature control. The error in concentration was estimated to be 5%. The diffusion times obtained at $\lambda_1 = 514$ nm may be corrected to the geometry factor, S, at $\lambda_1 = 488$ nm by

$$\tau_{488nm} = (w_{xy}^2{}_{(488)}/w_{xy}^2{}_{(514)})\tau_{514nm} \quad (5)$$

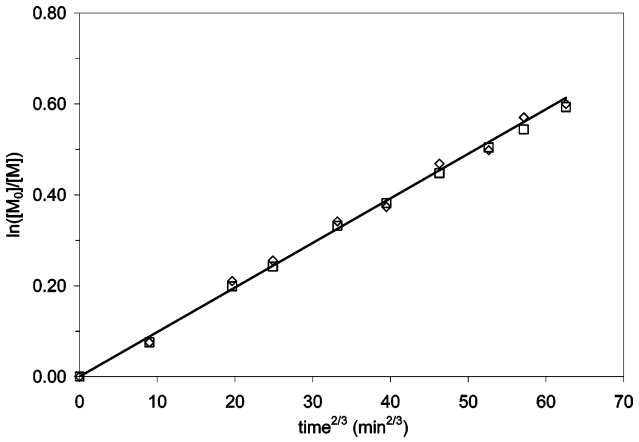

Figure 1. Semilogarithmic plot of monomer conversion followed by ^{1}H NMR (◇) and gas chromatography (□), vs $t^{2/3}$, during the synthesis of the P*n*BA$_{90}$-Br macroinitiator.

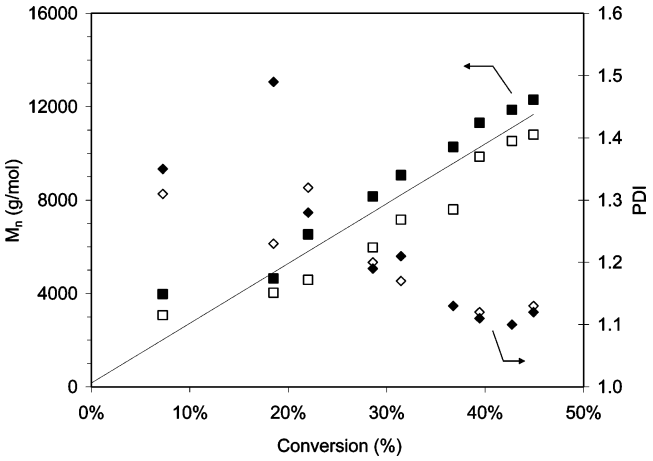

Figure 2. Evolution of the molecular weight (■, SEC; □, MALDI-TOF MS) and of the polydispersity index (PDI) with monomer conversion (◆, SEC; ◇, MALDI TOF MS) of the P*n*BA$_{90}$-Br macroinitiator. The straight line corresponds to the theoretical molecular weight.

The autocorrelation functions were evaluated by a homemade software fitting the data to eq 1 by a Levenberg−Marquart algorithm.[37] In order to determine the geometry of the laser focus, an aqueous solution of Rh6G was used as reference. The geometry parameter S was deduced for each cover slide applied for cmc determination after adjusting the pinhole and kept constant for the fitting of the experimental data for all subsequent measurements performed on the respective slide. The waist radii $w_{xy}(\lambda_1 = 488$ nm) = 205 nm and $w_{xy}(\lambda_2 = 514$ nm) = 246 nm were derived from the reference measurements taking advantage of the known diffusion coefficient of Rh6G in water[38] ($D = 4.18 \times 10^{-10}$ m^2/s). Optical saturation and photobleaching effects[39] were avoided by reducing the irradiance far below saturation until no change was observed in diffusion times during calibration and sample measurements. The detection volume $V_c = 2\pi w_{xy}^2 w_z$ was determined to be around 0.2 fL ($\lambda = 488$ nm) and 0.4 fL ($\lambda = 514$ nm). The F-test was exploited to verify the validity of a single-component ($K = 1$) or a two-component model ($K = 2$).

Results and Discussion

1. Synthesis and Molecular Characterization of the Diblock Copolymers. The diblock copolymers were synthesized by sequential monomer addition using ATRP for the polymerization of both blocks. In order to obtain block copolymers having a constant poly(*n*-butyl acrylate (P*n*BA) block length for different lengths of the poly(acrylic acid) (PAA) blocks, *n*-butyl acrylate (*n*BA) was polymerized first to yield a

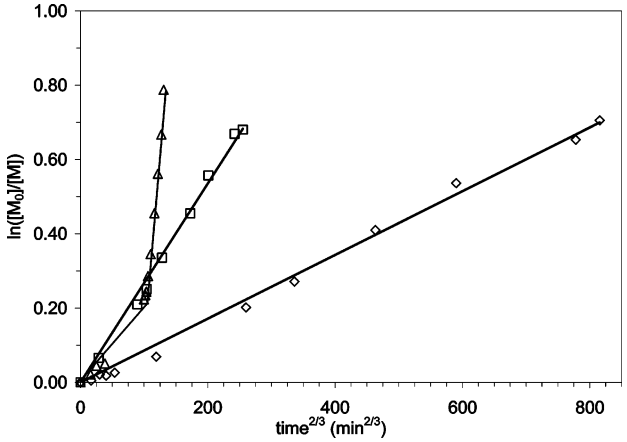

Figure 3. Semilogarithmic plot of monomer conversion followed by gas chromatography vs $t^{2/3}$ during the synthesis of P*n*BA$_{90}$−P*t*BA$_{33}$ (△) (after 17 h the temperature was raised from 40 to 60 °C); P*n*BA$_{90}$−P*t*BA$_{100}$ (□), and P*n*BA$_{90}$−P*t*BA$_{300}$ (◇).

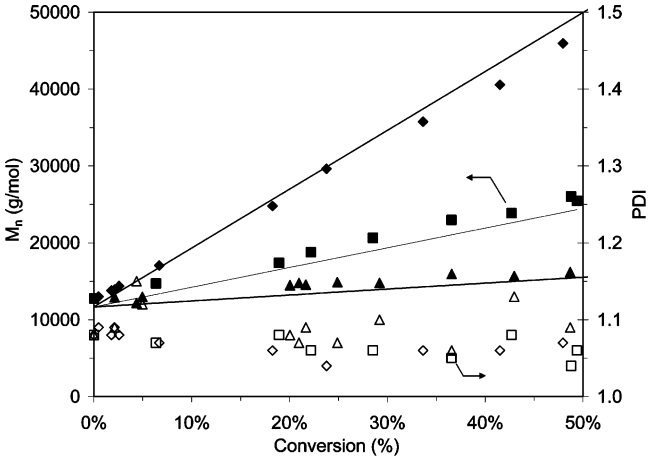

Figure 4. Evolution of the molecular weight (filled symbols) and of the polydispersity index (empty symbols) with monomer conversion of P*n*BA$_{90}$−P*t*BA$_{33}$ (▲, △), P*n*BA$_{90}$−P*t*BA$_{100}$ (■, □), and P*n*BA$_{90}$−P*t*BA$_{300}$ (◆, ◇) determined by SEC. The straight lines correspond to the theoretical molecular weights.

P*n*BA$_{90}$-Br macroinitiator. The evolution of conversion, plotted as ln([M]$_0$/[M]) vs $t^{2/3}$ (Figure 1), is in agreement with Fischer's theory[40] of the persistent radical effect. This observation together with a linear evolution of the number-average molecular weight, M_n, with conversion, a decrease of the polydispersity index with conversion (Figure 2), and a final polydispersity index close to 1.1 indicates a well-controlled polymerization process. The reaction was quenched at only 45% conversion in order to avoid termination reactions and thus to minimize the loss of Br end groups at the terminus of the P*n*BA block.

The diblock copolymers were then obtained by initiating the polymerization of *tert*-butyl acrylate (*t*BA) with the P*n*BA-Br macroinitiator. According to Figures 3 and 4, the polymerization of the second block is also well controlled in each case, and the polydispersity index remains below 1.1. Moreover, the final diblock copolymers initiated by P*n*BA$_{90}$-Br show no significant trace of residual homopolymer of P*n*BA (Figure 5), indicating an efficiency of the P*n*BA$_{90}$-Br macroinitiator close to 100%. This confirms that quenching the polymerization of the P*n*BA block at 45% conversion was efficient to minimize the loss of Br end groups. The molecular weights and polydispersity indices of the block copolymers are given in Table 2.

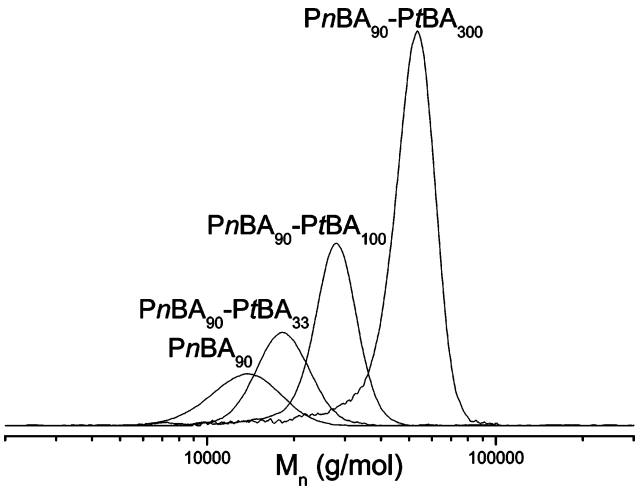

Figure 5. SEC eluograms of the macroinitiator, P*n*BA$_{90}$, and of the corresponding block copolymers.

The acid-catalyzed elimination of isobutylene from the P*t*BA blocks was then performed with trifluoroacetic acid in dichloromethane[41] to yield the final P*n*BA−PAA diblock copolymers. Hydrolysis with aqueous HCl in dioxane[42] was not used since it was found to partially hydrolyze the P*n*BA block.[43] With trifluoroacetic acid, at least 95% of the P*t*BA was converted into PAA. The characteristic peak of the *tert*-butyl group could indeed not be detected any more either with ^{1}H NMR (δ = 1.44 ppm, C(C*H*$_3$)$_3$; Figure 6) or with ^{13}C NMR (δ = 80.7, O−*C*(CH$_3$)$_3$ and δ = 28.5(O−C(*C*H$_3$)$_3$; Figure 7) after the reaction. Moreover, the PAA to P*n*BA ratio, as determined by ^{1}H NMR, fits rather well with the theoretical values (Table 2). Acidolysis of homo-P*n*BA under the same conditions did not indicate the formation of any detectable acrylic acid units according to ^{13}C NMR (i.e., the *C*═O peak at δ = 177.1 ppm characteristic of PAA units did not appear after the reaction, and only the *C*═O peak at δ = 175.0 ppm corresponding to P*n*BA units is visible). Thus, the acidolysis is selective and quantitative toward *t*BA units and does not alter the P*n*BA block.

As a conclusion, three narrowly distributed (PDI < 1.1) P*n*BA−PAA block copolymers having a constant P*n*BA block length (degree of polymerization, DP$_n$ = 90) and predefined PAA blocks were obtained in a well-controlled manner by ATRP. In addition, P*n*BA$_{100}$−PAA$_{150}$ was synthesized following a similar procedure. However, the rather high amount of ligand (PMDETA, which was shown to act as a transfer agent[44]) and of CuBr, as well as the high final conversion (70%), probably led to a partial loss of the bromine end groups of the P*n*BA$_{100}$ macroinitiator. As a consequence, this macroinitiator was not fully efficient, and pure P*n*BA$_{100}$−PAA$_{150}$ diblock was only obtained after elimination of the residual homo-P*n*BA$_{100}$ by Soxhlet extraction in cyclohexane (see Supporting Information for synthetic details). Differential scanning calorimetry of P*n*BA$_{90}$−PAA$_{100}$ revealed that the glass transition temperatures, T_g, of the P*n*BA$_{90}$ and of the PAA$_{100}$ blocks are −55 ± 1 and 85 ± 2 °C, respectively.

2. Aqueous Solution Properties. 2.1. Solubility and Potentiometric Titrations. The three block copolymers having the longest PAA block (DP$_{PAA}$ = 100−300) dissolve spontaneously at pH > 9 (α = 1) and stay soluble down to pH < 2.5 (α = 0) when back-titrated with HCl. In contrast, the polymer with the shortest block (DP$_{PAA}$ = 33) is insoluble at any pH (as long as no cosolvent is used) and will not be further discussed herein. Moreover, none of the protonated polymers (α = 0) dissolve spontaneously in pure water (under these conditions, pH ∼ 3.5).

Table 2. Molecular Characteristics of the Different P*n*BA−P*t*BA Block Copolymers

	$10^{-3}M_n$ (g/mol)			PDI	*t*BA (mol %)		PAA (mol %)[a]	
	theor	MALDI-TOF MS	SEC	SEC	theor	^{1}H NMR	^{1}H NMR	potentiometry
P*n*BA$_{90}$	11.7	12.9	12.7	1.09				
P*n*BA$_{100}$	12.3	12.5	15.3	1.07				
P*n*BA$_{90}$−P*t*BA$_{33}$	15.9	16.8	17.7	1.05	0.27	0.29	0.27	
P*n*BA$_{90}$−P*t*BA$_{100}$	24.3	24.7	25.6	1.07	0.52	0.54	0.50	0.47
P*n*BA$_{100}$−P*t*BA$_{150}$	32.0		33.7	1.04	0.60		0.56	0.57
P*n*BA$_{90}$−P*t*BA$_{300}$	50.4	51.4	47.2	1.07	0.77	0.78	0.78	0.71

[a] The molar percentage of PAA was determined by ^{1}H NMR in MeOD or THF as well as by potentiometry after hydrolysis of the diblocks. Values obtained by potentiometry are probably underestimated because of a few percents of adsorbed water in the polymer.

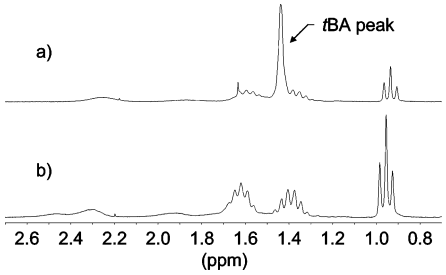

Figure 6. ^{1}H NMR spectra of (a) P*n*BA$_{90}$−P*t*BA$_{100}$ in $CDCl_3$ and (b) P*n*BA$_{90}$−PAA$_{100}$ in $CDCl_3$/MeOD (85/15 v/v).

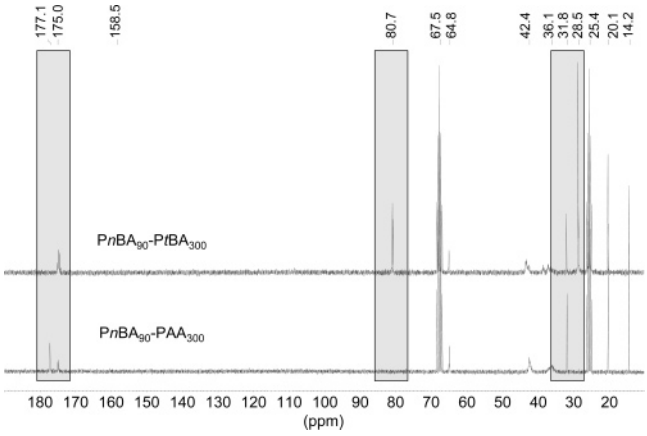

Figure 7. ^{13}C NMR spectra ([D_8]THF) of P*n*BA$_{90}$−P*t*BA$_{300}$ and P*n*BA$_{90}$−PAA$_{300}$.

As a quantitative example, a turbid suspension of P*n*BA$_{90}$−PAA$_{100}$ (containing 0.1 M NaCl), titrated from pH ∼ 2.5 by NaOH (with 0.1 M NaCl), only becomes transparent for pH > 4.7 ($\alpha \sim 0.2$). We assume that this is due to the rather poor solubility of protonated PAA. The structure of these turbid solutions will be investigated in the subsequent publication in this series.[24]

The study of the evolution of the pH of the block copolymers with the degree of ionization, $\alpha = [COO^-,Na^+]/[COOH]_0$ (ratio of ionized AA units), was carried out at a concentration of 1 g/L in the presence of a constant salt concentration of 0.1 M NaCl (added after dissolution of the polymer). The titrations yield apparent pK_a values (i.e., pH at $\alpha = 0.5$) between 5.5 and 5.7 (Figure 8). These values are considerably lower than those for linear[45,46] and star-shaped PAA[46] as well as for P*n*BA$_{90}$−PAA$_{150}$[47] in the absence of salt, reported to be between 6.3 and 6.5. However, they agree well with the value obtained for PAA titrated in the presence of 0.1 M NaCl (pK_a = 5.4).[48] This may be explained by the fact that, in the absence of salt, the negative charges created upon deprotonation of some AA units make the subsequent deprotonation of more AA units more and more difficult. In the presence of a sufficient amount of salt, those charges are screened, facilitating the deprotonation of all AA units.

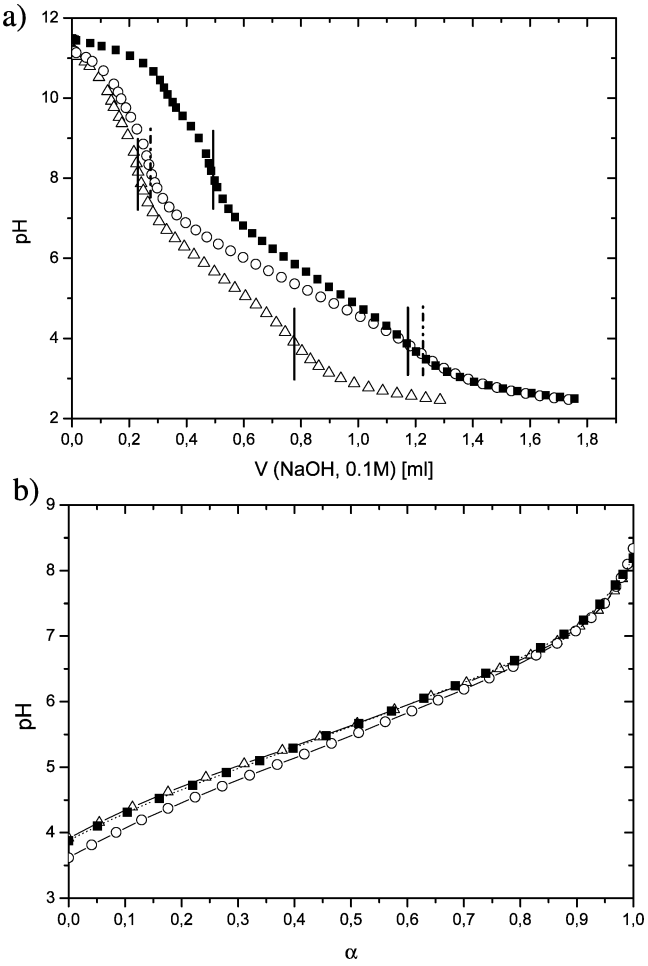

Figure 8. Potentiometric titration of ∼10 mg of P*n*BA$_{90}$−PAA$_{100}$ (△), P*n*BA$_{100}$−PAA$_{150}$ (■), and P*n*BA$_{90}$−PAA$_{300}$ (○) with aqueous HCl (0.1 and 0.1 M NaCl) starting from pH ∼ 11, in the presence of 0.1 M NaCl, and at a polymer concentration of 1 g/L. (a) Titration curves; equivalence points are indicated by vertical lines. (b) Dependence of pH on degree of ionization.

On closer inspection, the apparent pK_a of the block copolymer having the longest PAA block is slightly lower than that of the other polymers. It has been previously shown that the apparent pK_a of star-shaped PAA is decreasing with increasing arm length as the mean segment density within the star decreases and thus the osmotic pressure on the confined counterions is lowered.[46] Considering the amphiphilic character of our block copolymers, this may indeed reflect the presence of star-shaped micelles with PAA corona in aqueous solutions rather than single block copolymer chains. The existence of star-shaped micelles will be demonstrated in a subsequent publication.[24]

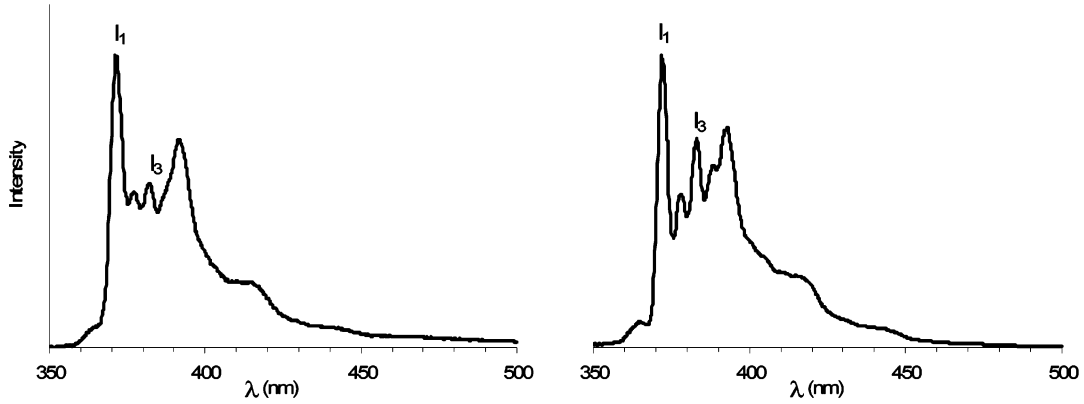

Figure 9. Emission spectrum of pyrene in an aqueous solution of P*n*BA$_{90}$−PAA$_{300}$ (0.1 M NaCl, 0.01 M TRIS, pH ∼ 9−10) at $c = 10^{-10}$ mol/L (left) and $c = 10^{-4}$ mol/L (right).

Table 3. Critical Micelle Concentrations of the Block Copolymers at pH ∼ 9−10 (α = 1) and Respective Number-Average Hydrodynamic Radii of Micelles

		cmc (pyrene fluorescence)		cmc (FCS)		
	c_{NaCl} (mol/L)	(10^{-8} mol/L)	(mg/L)	(10^{-8} mol/L)	(mg/L)	$\langle R_h \rangle_n$[a] (FCS) (nm)
P*n*BA$_{90}$−PAA$_{100}$	0			2.4 ± 1.1[b]	0.45 ± 0.2[b]	28 ± 3[b]
				3.6 ± 1.7[c]	0.65 ± 0.3[c]	23 ± 2[c]
	0.1	4.5 ± 2.5	0.8 ± 0.5	12 ± 1.7[c]	4.4 ± 0.3[c]	21 ± 2[c]
P*n*BA$_{100}$−PAA$_{150}$	0			1.9 ± 0.9[b]	0.45 ± 0.2[b]	36 ± 2[b]
	0.1	2 ± 1	0.5 ± 0.3			
P*n*BA$_{90}$−PAA$_{300}$	0	2 ± 1.5	0.7 ± 0.5	1.4 ± 0.6[b]	0.45 ± 0.2[b]	55 ± 2[b]
				(13 ± 1.4)[c]	(4.7 ± 0.5)[c]	(79 ± 3)[c]
	0.1	2 ± 1	0.7 ± 0.4	2.0 ± 0.6[c]	0.7 ± 0.2[c]	39 ± 3[c]

[a] Average of three independent experiments at 0.45 g/L for P*n*BA$_{90}$−PAA$_{100}$ and P*n*BA$_{90}$−PAA$_{300}$ and at 1.13 g/L for P*n*BA$_{100}$−PAA$_{150}$. [b] Evaluated with Rh6G as fluorescent tag. [c] Evaluated with ORB as fluorescent tag.

Finally, the content of AA units per copolymer determined by potentiometric titration fits well with the composition of the block copolymers (Table 2), taking into account that this content may be underestimated because of a small percentage of water in the polymer.

2.2. Determination of the Critical Micelle Concentration (cmc). Pyrene Fluorescence Spectroscopy. The onset of micelle formation of saline solutions of our amphiphilic block copolymers (0.1 M NaCl and α = 1) was evaluated using steady-state fluorescence spectroscopy of pyrene. This approach has proven to be a versatile method to determine the onset of micelle formation of block copolymer amphiphiles in aqueous media.[23,29,30,49,50] In this approach, the ratio between the intensities of the first (I_1) and the third (I_3) vibrational bands of the pyrene emission spectrum decreases with the polarity of the medium in which pyrene is dissolved (Figure 9). I_1/I_3 remains constant (∼1.7−1.8) at polymer concentrations $c < 4.5 \times 10^{-8}$ mol/L, below which pyrene is in aqueous environment, indicating the absence of micelles. As soon as micelles are formed, pyrene migrates into the hydrophobic core (or the core−corona interface) and I_1/I_3 decreases. The cmc (Table 3) was determined as the intersection between the plateau at $I_1/I_3 \sim 1.7-1.8$ and the tangent of the decrease of I_1/I_3 vs concentration in Figure 10. The cmc of P*n*BA$_{90}$−PAA$_{300}$ was also determined at pH ∼ 9 (α ∼ 1) in the absence of salt, furnishing the same onset of micelle formation as in saline solutions.

Here, it has to be highlighted that pyrene fluorescence spectroscopy may only give an upper estimate of the cmc. Indeed, the polymer concentration at which I_1/I_3 starts to decrease is equal to 10^{-8} mol/L, which is lower than the pyrene concentration (5×10^{-7} mol/L). The molar concentration of micelles is even lower by 2 orders of magnitude, taking into account the aggregation number of the micelles, which was determined to be around 200−300 for all polymers at polymer concentrations of 10 g/L.[24] Consequently, a partitioning of the pyrene molecules between the water solution and the micelles at low concentrations could also lead to high values of I_1/I_3. Thus, in order to corroborate the steady-state fluorescence spectroscopy results, fluorescence correlation spectroscopy experiments were performed.

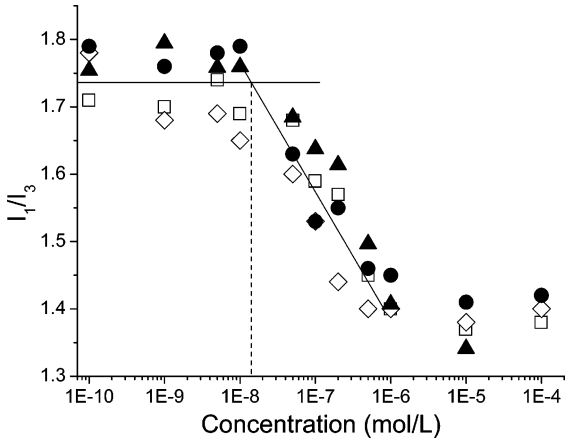

Figure 10. Determination of the cmc using fluorescence spectroscopy of pyrene: P*n*BA$_{90}$−PAA$_{100}$ (□), P*n*BA$_{100}$−PAA$_{150}$ (●), and P*n*BA$_{90}$−PAA$_{300}$ (◇) at pH ∼ 10 and 0.1 M NaCl and of P*n*BA$_{90}$−PAA$_{300}$ (▲) at pH ∼ 9 without added salt or buffer.

Fluorescence Correlation Spectroscopy (FCS). The onset of micelle formation and the hydrodynamic radii of the micelles were also determined by FCS. Instead of using covalently dye-labeled polymers,[51] the micelles were fluorescently tagged with the cationic laser dyes Rhodamine 6G perchlorate (Rh6G) in the absence of added salt and octadecylrhodamine B (ORB) in the absence and presence of added salt. This approach has been shown to be a convenient method to study the aggregation

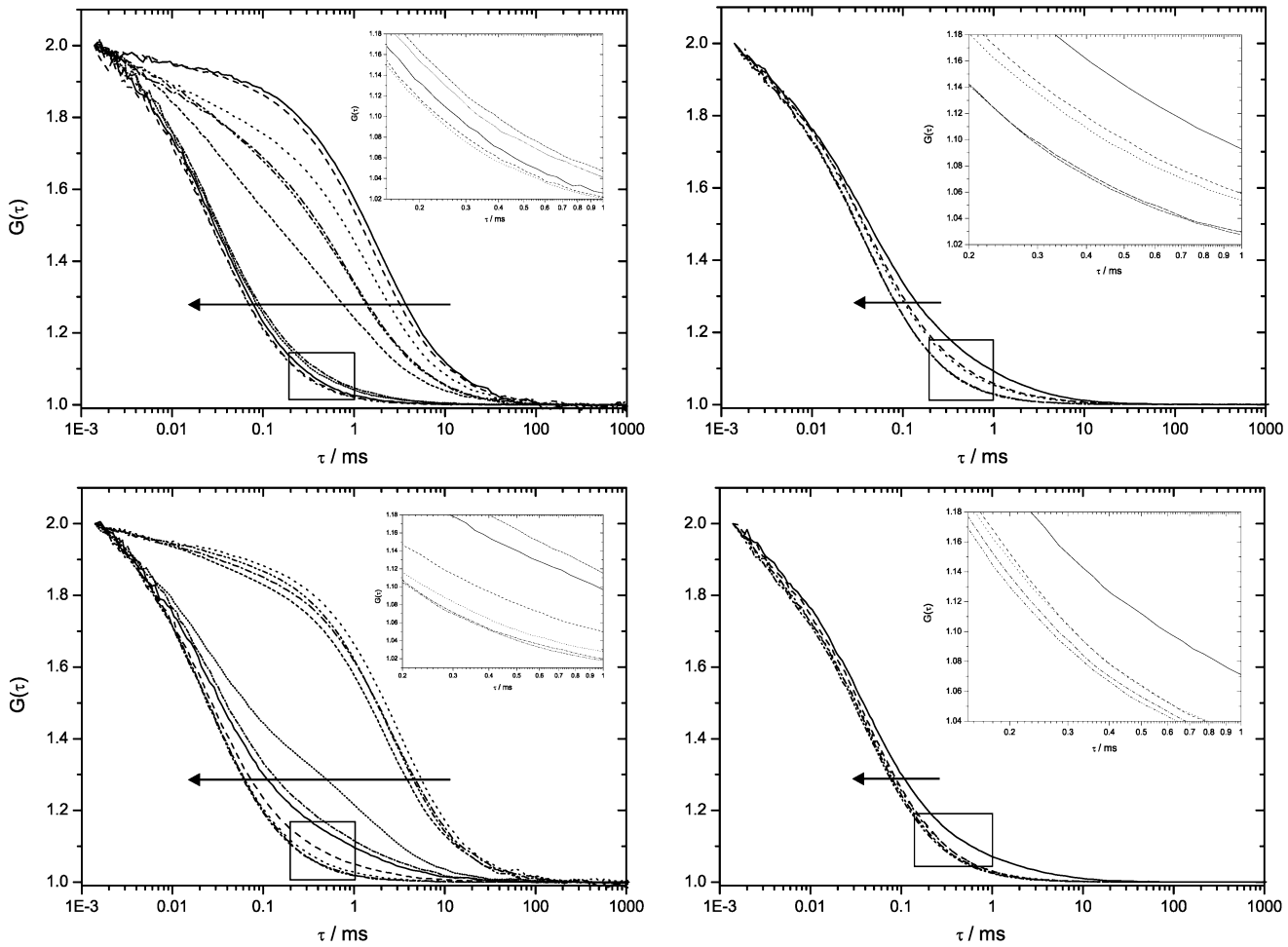

Figure 11. Representative normalized autocorrelation functions of P*n*BA$_{90}$−PAA$_{100}$ (top) and P*n*BA$_{90}$−PAA$_{300}$ (below) for decreasing polymer concentrations (pH ∼ 9.5, α ∼ 1) at two different dye concentrations: $c_{1,0}$(Rh6G) = 2.0 × 10^{-8} (left) and $c_{2,0}$(Rh6G) = 1.0 × 10^{-9} (right). Excitation at λ = 488 nm. The arrows represent the direction of decreasing polymer concentrations (in mg/L) in the following order: 450, 90, 45, 9.0, 4.5, 2.3, 0.68, 0.45, 0.23, 0.090, 0 (top right); 475, 90, 45, 9.0, 2.3, 0.90, 0.68, 0.45, 0.23, 0.090, 0 (bottom right); and 2.3, 0.90, 0.68, 0.45, 0.23 (left, top and bottom). The inserts are magnifications of box sections.

behavior of low-molecular-weight surfactants[52] as well as for amphiphilic block copolymer systems.[20,25,53,54]

Experiments at Low Ionic Strength Using Rh6G. The poorly water-soluble Rh6G proved to be a suitable dye for our system in the absence of added salt, as it binds sufficiently to the negatively charged micelles, exhibiting high quantum yields and low triplet fractions (<15%). In contrast, rhodamine B and cresyl violet provided too poor binding capabilities to be suitable as fluorescent tags. Indeed, cresyl violet exhibited the worst affinity to the micelles. This is noteworthy, as cresyl violet does not significantly differ from Rh6G with respect to its charge and skeletal structure. The significant difference in binding capabilities is attributed to the more strongly pronounced hydrophobic nature of Rh6G as an ethyl ester derivative of rhodamine B. Thus, besides electrostatic interactions the hydrophobic interactions seem to be essential to bind sufficiently to micelles. The relevance of Rh6G's hydrophobicity to bind efficiently to charged particles in aqueous media is well documented.[55−57] Unexpectedly, ORB, a strongly hydrophobic dye, also exhibited only poor binding efficiencies in the absence of salt, whereas it was reported to bind efficiently to amphiphilic block copolymer micelles with PMAA shell in saline solutions.[54]

Representative experimental autocorrelation functions (ACF) for different polymer concentrations are shown in Figure 11. Experiments were conducted at two different dye concentrations: $c_{1,0}$(Rh6G) = 2.0 × 10^{-8} mol/L and $c_{2,0}$(Rh6G) = 1.1 × 10^{-9} mol/L. Considering the molar mass of the polymers, the polymer molar concentration assessed ranges from 0.7 × 10^{-9} to 5 × 10^{-5} M. In terms of molar concentration of micelles, however, this is in order of magnitudes lower (3 × 10^{-12} M < $c_{micelle}$ < 1 × 10^{-7} M) as their aggregation number were determined to be N_{agg} = 186, 192, and 303 for P*n*BA$_{90}$−PAA$_{300}$, P*n*BA$_{100}$−PAA$_{150}$, and P*n*BA$_{90}$−PAA$_{100}$, respectively.[24] Therefore, the molar micelle concentration becomes lower than the dye concentration at polymer mass concentrations *c*(polymer) ≤ 50 mg/L, corresponding to molar micelle concentrations $c_{micelles}$ ≤ 10 nM. Experiments with the lower dye concentration were therefore conducted in order to apply a more reasonable micelles-to-dye molar ratio.

Figure 11 shows three major concentration regimes. At high concentrations (*c* > 90 mg/L) a single slow diffusive process determines the ACFs. At an intermediate concentration regime, two diffusive processes dominate the ACFs, revealing significantly different diffusion times. At polymer concentrations *c* < 0.45 mg/L and *c* < 0.68 mg/L at dye concentrations $c_{1,0}$(dye) = 1.0 × 10^{-8} mol/L and $c_{2,0}$(dye) = 1.1 × 10^{-9} mol/L, respectively, no contribution of a slow component is evident for P*n*BA$_{90}$−PAA$_{100}$ and P*n*BA$_{90}$−PAA$_{300}$. This holds also true for P*n*BA$_{100}$−PAA$_{150}$.

By fitting the experimental ACFs to eq 1, these concentration regimes may be quantified by plotting the diffusion times as a function of polymer concentration as shown in Figure 12. At

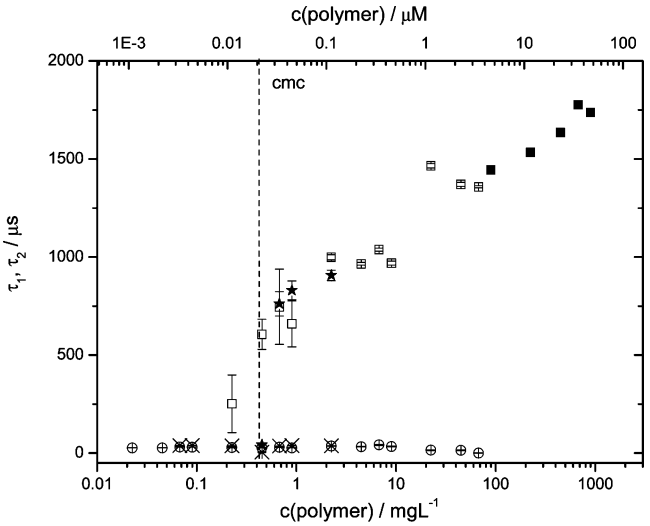

Figure 12. Logarithmic plot of translational diffusion times vs polymer concentration (mass and molar concentration, bottom and top axis, respectively). Fast diffusive time, τ_1 (○), and slow diffusive time, τ_2 (two-component model (□), and one-component model (■)), for P*n*BA$_{90}$−PAA$_{100}$ obtained at $\lambda = 488$ nm ($c_{1,0}$(Rh6G) $= 2.0 \times 10^{-8}$ mol/L) and the respective values τ_1 (×) and τ_2 (★) obtained by measurements at $\lambda = 514$ nm ($c_{2,0}$(Rh6G) $= 1.1 \times 10^{-9}$ mol/L). (All symbols were attributed error bars, which may affect the representation of the open ones.)

polymer concentrations $c > 90$ mg/L, the ACFs were well fitted to a one-component model ($K = 1$), yielding diffusion times $\tau_2 = 1700-2500$ μs (depending on the polymer). This clearly indicates the presence of large aggregates, i.e., micelles. At the intermediate concentration regime (0.3 mg/L $< c <$ 70 mg/L) eq 1 was fitted to the experimental data applying a two-component model ($K = 2$). In this region, free dye molecules with a diffusion time $\tau_1 = 26 \pm 2$ μs and aggregates with diffusion times $\tau_2 = 1400-1850$ μs (at the beginning of the two-component region, depending on the polymer) coexist. Finally, at very low block copolymer concentration, $c < 0.45$ mg/L, fits were satisfactory only when applying a one-component model ($K = 1$) resulting in the diffusion time of the free dye molecule, τ_1.

In a second step of data analysis, the respective diffusion times for the free dye (τ_1(Rh6G, 488 nm) $= 26$ μs and τ_1(Rh6G, 514 nm) $= 37$ μs)—as derived from calibration measurements—were fixed at their known values, fitting the experimental autocorrelation data with a reduced number of fitting variables to grant for better accuracy in evaluated parameters.

The evolution of the diffusion times with polymer concentration for all polymers is summarized in Figure 13 (top). Here, only the slow diffusion times (τ_2) are represented within the two-component region. Calibration of the detection volume also enabled to calculate the diffusion coefficient and the number-average hydrodynamic radius, R_h (eq 7) (Figure 13, middle). Finally, the fraction of dye molecules bound to polymer was determined as the respective fitting parameter whenever the two-component model applied (Figure 13, bottom). It is set to zero at the lowest concentration when a single diffusion time corresponding to free dye is observed and respectively assigned to unity whenever only diffusion times corresponding to micelles are evident.

As it becomes evident from Figure 12 and Figure 13 (middle), the number-average hydrodynamic radii of the fluorescent-tagged species increases at a polymer concentration of ca. 0.23 mg/L from 0.6 to 2.3, 4.9, and 10 nm for P*n*BA$_{90}$−PAA$_{100}$, P*n*BA$_{100}$−PAA$_{150}$, and P*n*BA$_{90}$−PAA$_{300}$, respectively. These

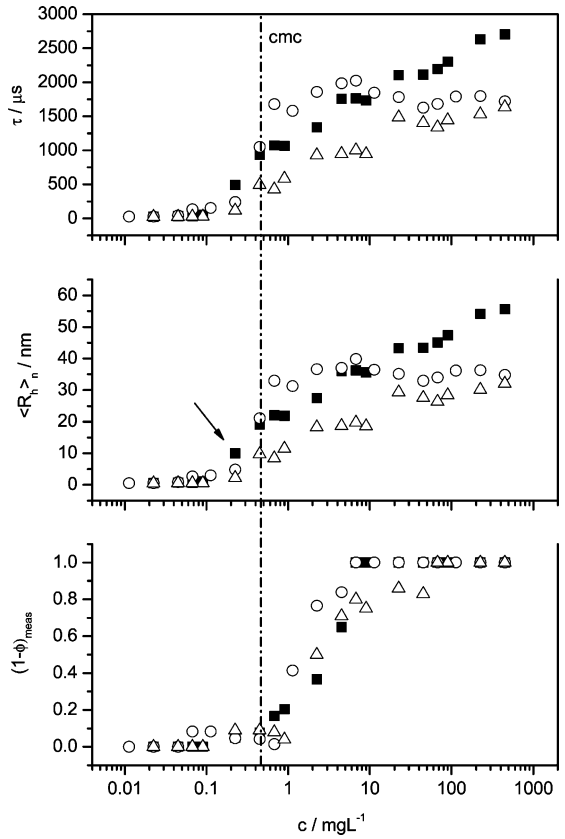

Figure 13. Evolution of translational diffusion times (top), number-average hydrodynamic radii (middle), and fraction of fluorescent-tagged micelles (bottom) for P*n*BA$_{90}$−PAA$_{300}$ (■), P*n*BA$_{100}$−PAA$_{150}$ (○), and P*n*BA$_{90}$−PAA$_{100}$ (△) at pH ∼ 9.5 with no added salt ($\lambda = 488$ nm, $c_{1,0}$(Rh6G) $= 2.0 \times 10^{-8}$ mol/L). The vertical dashed line indicates the cmc. Diffusion times assigned to dye attached to single chains are highlighted by an arrow.

hydrodynamic radii roughly correspond to those of single polymer chains, assuming that the P*n*BA segments are collapsed and PAA segments are stretched to 1/4 to 1/2 of their contour length, $L_c = DP \times l_{mon}$ (where $l_{mon} = 0.25$ nm is the length of a monomer unit and DP denotes the degree of polymerization of the PAA block). This indicates that no micellar aggregates are formed at this concentration. Moreover, explicit contribution of a second slow diffusive process to the ACFs is only evident at polymer concentrations above 0.45 or 0.68 mg/L at $c_{1,0}$(Rh6G) $= 2.0 \times 10^{-8}$ mol/L or $c_{2,0}$(Rh6G) $= 1.1 \times 10^{-9}$ mol/L, respectively (see Figure 11, insets). The exiguous discrepancy between the two dye concentrations is attributed to a shifting of the dye−micelle association equilibrium to the dissociated state, worsening the detection limit for the slower diffusion time, due to a lower fraction of labeled micelles.

The onset of micelle formation is therefore determined as the minimum concentration where the second diffusion time of the aggregates is higher than the value expected for single chains and explicitly contributes to the ACFs. Thus, the cmc in the absence of added salt is assigned to be 0.45 mg/L for all polymers assessed herein.

The number-average hydrodynamic radii obtained at $c \gg$ cmc (Table 3) very well coincide with the *z*-average values obtained by dynamic light scattering (DLS) at comparable concentrations: $\langle R_h \rangle_z = 30$ nm (P*n*BA$_{90}$−PAA$_{100}$) and $\langle R_h \rangle_z = 61$ nm (P*n*BA$_{90}$−PAA$_{300}$).[24] However, a distinct dependence of the hydrodynamic radii on dilution is observed in all cases. Indeed, attempts to fit the experimental data according to a two-component model, where both diffusion times were fixed to

the respective values of free dye and micelles of constant size, failed in all cases (see Supporting Information). This excludes apparent diffusion times as a fitting artifact due to alleged fractions. As this notable observation may be also attributed to the binding properties of the applied fluorescent probe, further experiments were accomplished using highly hydrophobic octadecylrhodamine B (ORB) as the fluorescent tag, which was reported to strongly bind to micelles with PMAA corona.[58] Their outcomes are provided in the following.

Experiments at Low Ionic Strength Using ORB. As highlighted above, ORB exhibits a much poorer binding to our micelles compared to Rh6G. Even at the highest polymer concentration the diffusion time corresponding to the free dye τ_1(ORB, 514 nm) = 37 ± 1 μs contributed up to $\phi_1 = 10\%$ to the ACFs. Furthermore, micelles tagged with ORB showed a significant lower fluorescent brightness and higher triplet fractions (15% < T < 24%) compared to Rh6G as fluorescent probe. This resulted in poor signal-to-noise ratios and a higher error for fast diffusive processes that may be convoluted with the triplet relaxation. Despite the rather poor performance, P*n*BA$_{90}$−PAA$_{300}$ and P*n*BA$_{90}$−PAA$_{100}$ solutions without added salt were studied using ORB as a fluorescence probe in order to seize the impact of the fluorescent tag on the apparent diffusion times assessed by FCS.

The significant decrease of the diffusion times with decreasing polymer concentration is, however, also evident with ORB (see Figure 14), which is consistent with measurements performed with Rh6G as the fluorescent tag (vide supra). Furthermore, the onset of micelle formation is obvious at 0.65 and 4.7 mg/L for P*n*BA$_{90}$−PAA$_{100}$ and P*n*BA$_{90}$−PAA$_{300}$, respectively (Table 3). For the polymer with the short hydrophilic block we find a good agreement for the cmc and the hydrodynamic radius of the micelles determined with the two different dyes. The polymer with the long hydrophilic block in measurements with ORB as fluorescent label has a higher cmc and shows larger hydrodynamic radii than with Rh6G. We attribute these differences to the fact that ORB is not suited for highly charged hydrophilic systems as present in salt-free solutions. The preferred binding to the core−shell interface[58] may be hindered owing to the high incompatibility of the hydrophobic dye and the hydrophilic corona, i.e., prohibiting an efficient penetration of the micelles' corona by the fluorescent tag. This effect is less distinct with P*n*BA$_{90}$−PAA$_{100}$, where the corona is thinner. Furthermore, it has to be stressed that in the absence of added salt the ACFs are clearly dominated by a rather slow diffusion time (τ_1 = 650 μs, corresponding to a hydrodynamic radius of 9.3 nm) at concentrations well below the assigned cmc. As this diffusion time is also apparent in aqueous ORB solution in the absence of any polymer (c(ORB) = 1 nM, see Figure 14, bottom), this diffusion time is attributed to aggregates of dye molecules. Nevertheless, the decline of R_h with decreasing polymer concentration is confirmed with ORB as fluorescent probe.

In the regime of low ionic strength the hydrophobic dye ORB can only be used for block copolymers with a short hydrophilic block. Otherwise, the hydrophobic interaction between dye and polymer is hindered, and no reliable FCS investigation is possible. In contrast, the ionic dye Rh6G can label both polymers sufficiently.

Experiments at High Ionic Strength. In the regime of high ionic strength the charges of the hydrophilic block are screened. Hence, an effective electrostatic interaction between dye and polymer is not possible, and the ionic dye Rh6G is not suitable for labeling the micelles. As expected, we found even at high

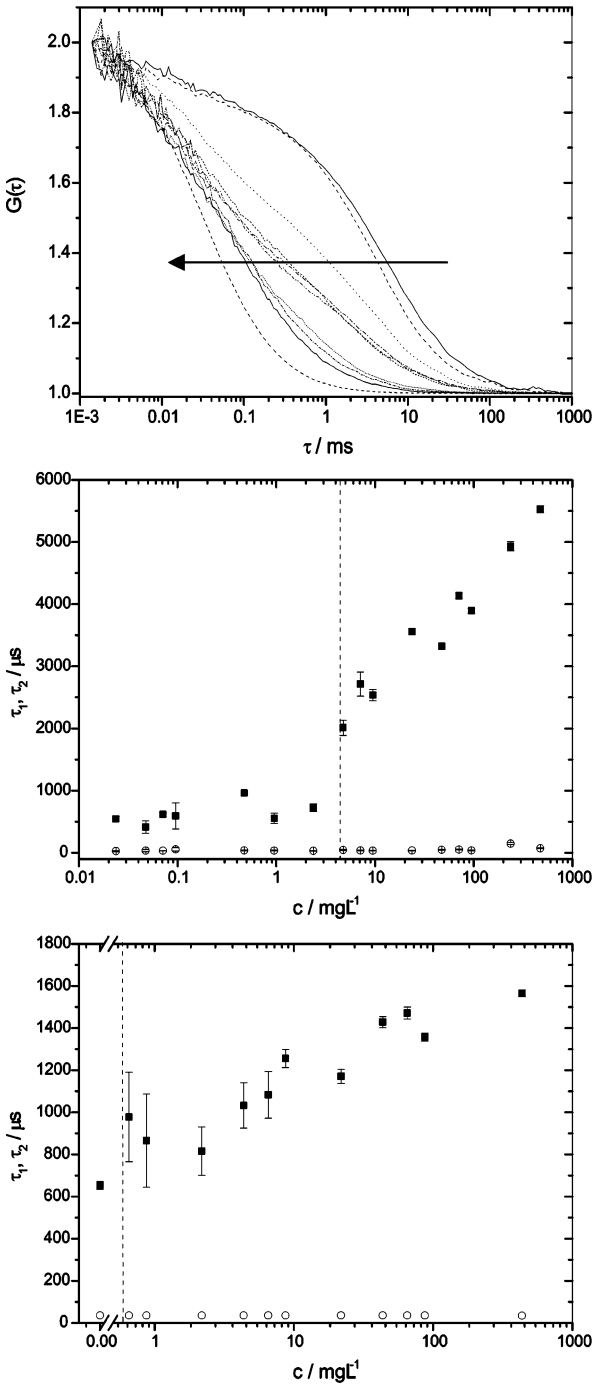

Figure 14. Normalized autocorrelation functions for decreasing polymer concentration in the absence of added salt for P*n*BA$_{90}$−PAA$_{300}$ (c_0(ORB) = 1.0 × 10^{-9} mol/L, top). The arrow indicates the decreasing polymer concentration (in mg/L) in the following order: 711, 237, 47, 9.5, 7.1, 4.7, 2.4, 0.90, and 0. Evolution of translational diffusion times with polymer concentration in the absence of added salt for P*n*BA$_{90}$−PAA$_{300}$ (middle) and P*n*BA$_{90}$−PAA$_{100}$ (bottom). The vertical dashed lines indicate the onset of micelle formation.

polymer concentrations no interaction between Rh6G and the polymer micelles. Although ORB exhibited a significantly lower fluorescent brightness and higher triplet fractions compared to Rh6G, it could be used for experiments at high ionic strength. Indeed, the binding of ORB to the polymer in the presence of added salt was slightly enhanced compared to the case at low ionic strength. Quantitatively, the diffusion time for free dye only contributed less than $\phi_1 < 5\%$ to the ACFs at the highest polymer concentration assessed. Furthermore, in contrast to the

case at low ionic strength no cluster formation of ORB molecules were evident in the presence of added salt. Only the diffusion time of the free dye molecules τ_1(ORB, 514 nm) = 37 ± 1 μs contributed to the ACFs in micellar solutions as well as in polymer-free aqueous solutions. Thus, experiments performed with ORB at high ionic strength allowed us to compare the results obtained at low and high ionic strength using the same dye. Experimental autocorrelation functions and the evolution of the diffusion times with decreasing polymer concentration for P*n*BA$_{90}$−PAA$_{300}$ and P*n*BA$_{90}$−PAA$_{100}$ in saline solutions are presented in Figure 15. The onsets of micelle formation are evident at $c = 0.7$ mg/L (P*n*BA$_{90}$−PAA$_{300}$) and $c = 4.4$ mg/L (P*n*BA$_{90}$−PAA$_{100}$).

In contrast to the situation in the absence of added salt, the diffusion times do not decrease significantly with decreasing polymer concentration. Moreover, the determined hydrodynamic radii at $c \gg$ cmc (Table 3), either with or without added salt, reflect the expected contraction of the ionic corona due to screened charges. The values are in reasonable agreement with the *z*-average values obtained by DLS measurements at the same ionic strength: $\langle R_h \rangle_z = 30$ nm (P*n*BA$_{90}$−PAA$_{100}$) and $\langle R_h \rangle_z = 51$ nm (P*n*BA$_{90}$−PAA$_{300}$).[24]

Discussion of the FCS Results. As stated above, we observe a significant dependence of the hydrodynamic radii on polymer concentration. Similar observations for micellar solutions of PIB−PMAA[25] and PVP−PEO,[58] studied by FCS and DLS, respectively, have already been reported earlier, although not further discussed. Very recently, Bendejacq et al. reported on highly asymmetric amphiphilic diblock copolymers, P(S-*stat*-AA)$_{\sim 20}$-*b*-PAA$_{\sim 200}$.[27] Small-angle neutron scattering proved that the corresponding micelles are dynamic when the molar amount of AA in the P(S-*stat*-AA) block reaches 50%, presenting an "apparent cmc" and showing a significant decrease in core size and aggregation number upon dilution like in our system. Such results appear to be in contrast to a closed association model that is generally used to describe micellization.

These results may be interpreted in terms of kinetic determined micellization. Theoretical studies by Besseling and Cohen Stuart,[59] Talanquer et al.,[60] and Nyrkova and Semenov[61,62] predict that the micellization of amphiphilic block copolymers with a liquidlike hydrophobic block is kinetically rather than thermodynamically controlled. Two activated processes have to be considered: unimer exchange dynamics, i.e., release and capture of amphiphilic unimers by micelles, and the nucleation process that is prerequisite for micelle formation (similar to crystallization). Indeed, the nucleation of micelles exerts the highest activation energies for these two processes owing to the high interfacial tension of the core−shell vicinity, which causes micelle formation and disintegration to be kinetically determined. Hence, the aggregation number and the onset of micelle formation may significantly differ from their thermodynamic quantities. In this respect, two consequences have to be highlighted herein: First, only "apperent cmcs" (kinetic cmc*) are experimentally accessible that can be considerably higher or lower than the thermodynamic cmc, depending on the experimental conditions. Second, a decrease of the unimer activity in solution by dilution furnish a pathway for micellar solutions to approach their thermodynamic state, i.e., aggregation number and molar concentration of micelles—provided that the unimer exchange dynamic is sufficiently fast (low activation barrier for unimer exchange). Indeed, a significant decrease of the aggregation number upon dilution is predicted, whereas the formation of new micelles is hindered due to the high activation barrier for nucleation.[63] The FCS results presented herein indeed

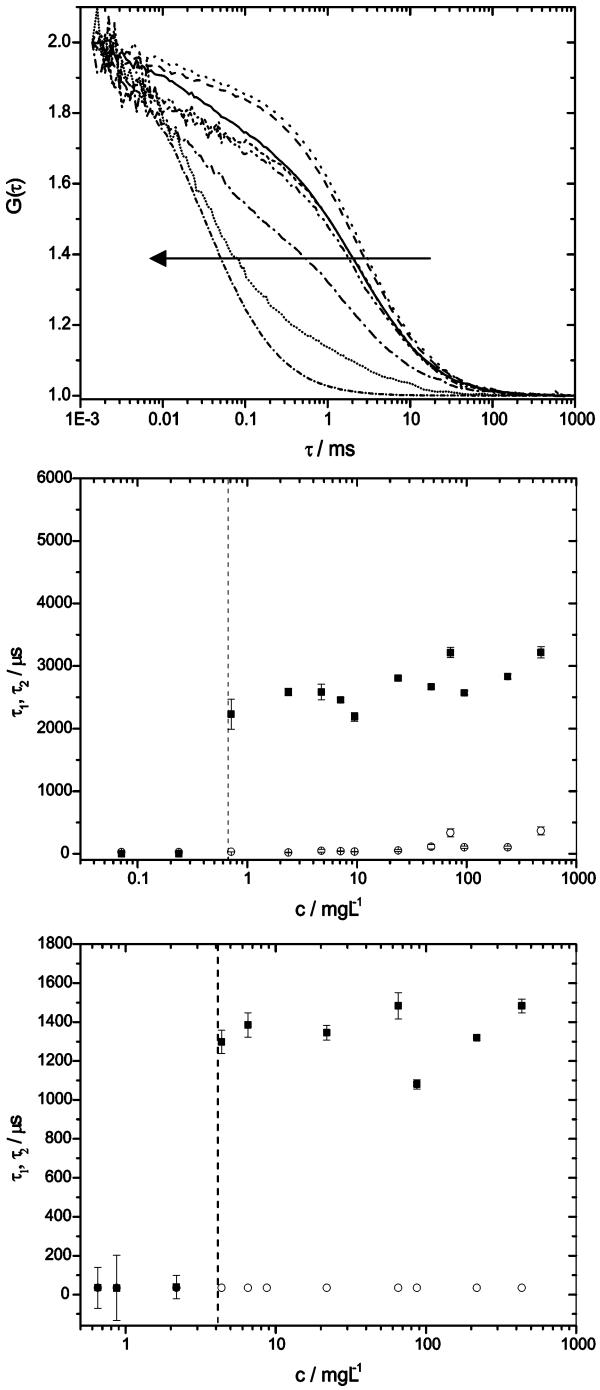

Figure 15. Normalized autocorrelation functions for decreasing polymer concentration in the presence of added salt *c*(NaCl) = 0.1 M for P*n*BA$_{90}$−PAA$_{300}$ (c_0(ORB) = 1.0×10^{-9} mol/L, top). The arrow indicates the decreasing polymer concentration in the following order: 711, 237, 47, 9.5, 4.7, 2.4, 0.71, and 0.24 mg/L. Evolution of translational diffusion times with polymer concentration in saline solution for P*n*BA$_{90}$−PAA$_{300}$ (middle) and P*n*BA$_{90}$−PAA$_{100}$ (bottom). The vertical dashed lines indicate the onset of micelle formation.

indicate such a predicted shrinking of micelles upon dilution at low ionic strength.

In saline solutions such a decrease in micellar's size is not evident, which is strongly indicative of a much slower unimer exchange dynamics in the presence of added salt. This is further sustained by a more detailed survey on the solution properties of the discussed micelles reported in the second contribution of this series.[24] Here, we provide sound experimental evidence that the polymer is readily dissolved in alkaline water under

the formation of narrowly distributed dynamic micelles in the absence of added salt,[24] whereas a dissolution of the polymer in saline aqueous solution is significantly hampered. Indeed, such micelles prepared in the presence of salt exhibit much higher hydrodynamic radii and do not approach the characteristics that are yielded for micelles prepared in the absence of salt.

Conclusions

P*n*BA−PAA diblock copolymers with a narrow molecular weight distribution and controlled composition (90−100 *n*BA units and 33−300 AA units) were successfully synthesized via ATRP. The block copolymers with PAA blocks $N_{AA} > 100$ dissolve readily in water at pH > 4.7 ($\alpha \sim 0.2$) without any cosolvent. This is noteworthy, considering the highly hydrophobic character of the long P*n*BA block.

Fluorescence correlation spectroscopy (FCS) provides hydrodynamic radii consistent with the formation of micelles. The cmc values in the absence and in the presence of added salt determined either by FCS or pyrene steady-state fluorescence spectroscopy are extremely low ($\sim 10^{-8}$ mol/L) and agree well within experimental error. They are in the same range as those of PIB−PMAA with comparable chain lengths of the hydrophobic block.[25] We were only able to determine an apparent (kinetic) cmc. Hence, it is not possible to draw quantitative conclusions on its dependence on block length or salinity.

The observed decrease of the micelle size with decreasing polymer concentration provides a first experimental hint for theories published recently, which consider the micelle formation of amphiphilic block copolymers as a kinetically controlled process. A more detailed discussion of all points predicted by the theoretical work exceeds the size of this contribution. For a deeper experimental verification of the theoretical predictions more time- and material-consuming experiments are necessary.

A detailed characterization of the structure and solution properties of the micelles presented herein under various conditions will be reported in a forthcoming paper.[24]

Acknowledgment. This work was supported by the European Union within the Marie Curie RTN POLYAMPHI and by DFG within SFB 481 and the ESF EUROCORES Programme SONS. We thank Rüdiger Ulbrich and Annette Krökel for NMR measurements, Denise Danz and Günther Jutz for MALDI-TOF MS measurements, Sabine Wunder, Xavier André, and Youyong Xu for SEC analysis, Harald Becker for his help with the GC, Mingfu Zhang for his kind advice for the synthesis of the block copolymers, and Oleg Borisov, Matthias Ballauff, and Christophe Chassenieux for helpful discussions.

Supporting Information Available: Synthesis and purification of the P*n*BA_{100}−PAA_{150} diblock copolymers; comparison of different FCS fitting procedures. This material is available free of charge via the Internet at http://pubs.acs.org.

References and Notes

(1) Zhang, L. F.; Eisenberg, A. *Science* **1995**, *268*, 1728−1731.
(2) Moffitt, M.; Eisenberg, A. *Macromol. Symp.* **1997**, *117*, 181−193.
(3) Allen, C.; Maysinger, D.; Eisenberg, A. *Colloids Surf., B* **1999**, *16*, 3−27.
(4) Förster, S.; Abetz, V.; Müller, A. H. E. *Adv. Polym. Sci.* **2004**, *166*, 173−210.
(5) Zhulina, E. B.; Borisov, O. V. *Macromolecules* **2005**, *38*, 6726−6741.
(6) Gohy, J. F. *Adv. Polym. Sci.* **2005**, *190*, 65−136.
(7) Cohen Stuart, M. A.; Hofs, B.; Voets, I. K.; de Keizer, A. *Curr. Opin. Colloid Interface Sci.* **2005**, *10*, 30−36.
(8) Babin, J.; Rodriguez-Hernandez, J.; Lecommandoux, S.; Klok, H.-A.; Achard, M.-F. *Faraday Discuss.* **2004**, *128*, 179−192.
(9) Chécot, F.; Lecommandoux, S.; Gnanou, Y.; Klok, H.-A. *Angew. Chem., Int. Ed.* **2002**, *41*, 1339−1343.
(10) Gnanou, Y.; Lecommandoux, S. *BIOForum Eur.* **2004**, *5*, 2−4.
(11) Burguière, C.; Pascual, S.; Bui, C.; Vairon, J.-P.; Charleux, B.; Davis, K. A.; Matyjaszeski, K.; Bétremieux, I. *Macromolecules* **2001**, *34*, 4439−4450.
(12) Gailard, N.; Guyot, A.; Claverie, J. *J. Polym. Sci., Part A: Polym. Chem.* **2003**, *41*, 684−698.
(13) Cao, T.; Munk, P.; Ramireddy, C.; Tuzar, Z.; Webber, S. E. *Macromolecules* **1991**, *24*, 6300−6305.
(14) Prochazka, K.; Kiserow, D.; Ramireddy, C.; Tuzar, Z.; Munk, P.; Webber, S. E. *Macromolecules* **1992**, *25*, 454−460.
(15) Qin, A. W.; Tian, M. M.; Ramireddy, C.; Webber, S. E.; Munk, P.; Tuzar, Z. *Macromolecules* **1994**, *27*, 120−126.
(16) Zhang, L.; Barlow, R. J.; Eisenberg, A. *Macromolecules* **1995**, *28*, 6055−66.
(17) Jada, A.; Hurtrez, G.; Siffert, B.; Riess, G. *Macromol. Chem. Phys.* **1996**, *197*, 3697−3710.
(18) Hurtrez, G.; Dumas, P.; Riess, G. *Polym. Bull. (Berlin)* **1998**, *40*, 203−210.
(19) Gohy, J.-F.; Willet, N.; Varshney, S.; Zhang, J.-X.; Jerome, R. *Angew. Chem., Int. Ed.* **2001**, *40*, 3214−3216.
(20) Loos, K.; Böker, A.; Zettl, H.; Zhang, A. F.; Krausch, G.; Müller, A. H. E. *Macromolecules* **2005**, *38*, 873−879.
(21) Bendejacq, D.; Ponsinet, V.; Joanicot, M. *Eur. Phys. J. E* **2004**, *13*, 3−13.
(22) Bendejacq, D.; Joanicot, M.; Ponsinet, V. *Eur. Phys. J. E* **2005**, *17*, 83−92.
(23) Pergushov, D. V.; Remizova, E. V.; Feldthusen, J.; Zezin, A. B.; Mueller, A. H. E.; Kabanov, V. A. *J. Phys. Chem. B* **2003**, *107*, 8093−8096.
(24) Colombani, O.; Ruppel, M.; Burkhardt, M.; Drechsler, M.; Gradzielski, M.; Schumacher, M.; Müller, A. H. E. *Macromolecules* **2007**, *40*, 4351−4362.
(25) Schuch, H.; Klingler, J.; Rossmanith, P.; Frechen, T.; Gerst, M.; Feldthusen, J.; Müller, A. H. E. *Macromolecules* **2000**, *33*, 1734−1740.
(26) Förster, S.; Hermsdorf, N.; Leube, W.; Schnablegger, H.; Regenbrecht, M.; Akari, S.; Lindner, P.; Böttcher, C. *J. Phys. Chem. B* **1999**, *103*, 6657−6668.
(27) Bendejacq, D. D.; Ponsinet, V.; Joanicot, M. *Langmuir* **2005**, *21*, 1712−1718.
(28) Barner-Kowollik, C.; Davis, T. P.; Heuts, J. P. A.; Stenzel, M. H.; Vana, P.; Whittaker, M. *J. Polym. Sci., Part A: Polym. Chem.* **2003**, *41*, 365.
(29) Dong, D. C.; Winnik, M. A. *Photochem. Photobiol.* **1982**, *35*, 17−21.
(30) Kalyanasundaram, K.; Thomas, J. K. *J. Am. Chem. Soc.* **1977**, *99*, 2039−2044.
(31) Böhmer, M. In *Single-Molecule Detection in Solution−Methods and Applications*, 1st ed.; Zander, C., Keller, R. A., Eds.; VCH-Wiley: Berlin, 2002; pp 145−183.
(32) Krichevsky, O.; Bonnet, G. *Rep. Prog. Phys.* **2002**, *65*, 251−297.
(33) Rigler, R. *Fluorescence Correlation Spectroscopy;* Springer: Berlin, 2001.
(34) Schwille, P. *Cell Biochem. Biophys.* **2001**, *34*, 383−408.
(35) Elson, E. L.; Magde, D. *Biopolymers* **1974**, *13*, 1−27.
(36) Van Craenenbroeck, E.; Engelborghs, Y. *J. Mol. Recognit.* **2000**, *13*, 93−100.
(37) Zettl, H.; Portnoy, Y.; Gottlieb, M.; Krausch, G. *J. Phys. Chem. B* **2005**, *109*, 13397−13401.
(38) Culbertson, C. T.; Jacobson, S. C.; Michael, Ramsey, J. *Talanta* **2002**, *56*, 365−373.
(39) Enderlein, J.; Gregor, I.; Patra, D.; Dertinger, T.; Kaupp, U. B. *ChemPhysChem* **2005**, *6*, 2324−2336.
(40) Fischer, H. *Chem. Rev.* **2001**, *101*, 3581−3610.
(41) Zhang, M.; Breiner, T.; Mori, H.; Müller, A. H. E. *Polymer* **2003**, *44*, 1449−1458.
(42) Davis, K. A.; Matyjaszewski, K. *Macromolecules* **2000**, *33*, 4039−4047.
(43) Müller, A. H. E.; Colombani, O.; Burkhardt, M.; Drechsler, M.; Fink, M.; Ruppel, M.; Gradzielski, M.; Pergushov, D. V. *Abstracts of Papers, 231st ACS National Meeting, Atlanta, GA, March 26−30, 2006* **2006**, COLL-387.
(44) Bednarek, M.; Tadeusz, B.; Kubisa, P. *Macromol. Chem. Phys.* **2000**, *201*, 58−66.
(45) Kern, W. *Biochem. Z.* **1939**, *301*, 338−56.
(46) Plamper, F. A.; Becker, H.; Lanzendörfer, M.; Patel, M.; Wittemann, A.; Ballauf, M.; Müller, A. H. E. *Macromol. Chem. Phys.* **2005**, *206*, 1813−1825.
(47) Eghbali, E.; Colombani, O.; Drechsler, M.; Müller, A. H. E.; Hoffmann, H. *Langmuir* **2006**, *22*, 4766−4776.

(48) Nagasawa, M.; Murase, T.; Kondo, K. *J. Phys. Chem.* **1965**, *69*, 4005−4012.
(49) Astafieva, I.; Khougaz, K.; Eisenberg, A. *Macromolecules* **1995**, *28*, 7127−7134.
(50) Astafieva, I.; Zhong, X. F.; Eisenberg, A. *Macromolecules* **1993**, *26*, 7339−7352.
(51) Bonne, T. B.; Ludtke, K.; Jordan, R.; Stepanek, P.; Papadakis, C. M. *Colloid Polym. Sci.* **2004**, *282*, 833−843.
(52) Zettl, H.; Portnoy, Y.; Gottlieb, M.; Krausch, G. *J. Phys. Chem. B* **2005**, *109*, 13397−13401.
(53) Erhardt, R.; Zhang, M. F.; Böker, A.; Zettl, H.; Abetz, C.; Frederik, P.; Krausch, G.; Abetz, V.; Müller, A. H. E. *J. Am. Chem. Soc.* **2003**, *125*, 3260−3267.
(54) Humpolickova, J.; Prochazka, K.; Hof, M.; Tuzar, Z.; Spirkova, M. *Langmuir* **2003**, *19*, 4111−4119.
(55) Arbeloa, F. L.; Ojeda, P. R.; Arbeloa, I. L. *J. Chem. Soc., Faraday Trans.* **1988**, *84*, 1903.
(56) Arbeloa, F. L.; Martinez, J. M. H.; Arbeloa, T. L.; Arbeloa, I. L. *Langmuir* **1998**, *14*, 4566−4573.
(57) Charreyre, M. T.; Zhang, P.; Winnik, M. A.; Pichot, C.; Graillat, C. *J. Colloid Interface Sci.* **1995**, *170*, 374−382.
(58) Martin, T. J.; Prochazka, K.; Munk, P.; Webber, S. E. *Macromolecules* **1996**, *29*, 6071−6073.
(59) Besseling, N. A. M.; Cohen Stuart, M. A. *J. Chem. Phys.* **1999**, *110*, 5432−5436.
(60) Talanquer, V.; Oxtoby, D. W. *J. Chem. Phys.* **2000**, *113*, 7013−7021.
(61) Nyrkova, I. A.; Semenov, A. N. *Faraday Discuss.* **2005**, *128*, 113−127.
(62) Nyrkova, I. A.; Semenov, A. N. *Macromol. Theory Simul.* **2005**, *14*, 569−585.
(63) Nyrkova, I. A.; Semenov, A. N. *Eur. Phys. J. E* **2005**, *17*, 327−337.

MA0609578